

C-terminal Recognition by 14-3-3 Proteins for Surface Expression of Membrane Receptors*

Received for publication, July 12, 2005, and in revised form, August 24, 2005 Published, JBC Papers in Press, August 24, 2005, DOI 10.1074/jbc.M507559200

Brian Coblitz[‡], Sojin Shikano^{†1}, Meng Wu[‡], Sandra B. Gabelli[§], Lisa M. Cockrell[¶], Matt Spieker[‡], Yoshiro Hanyu^{||}, Haian Fu[¶], L. Mario Amzel[§], and Min Li^{†1}

From the [‡]Department of Neuroscience and the High Throughput Biology Center and the [§]Department of Biophysics and Biophysical Chemistry, School of Medicine, Johns Hopkins University, Baltimore, Maryland 21205, the [¶]Department of Pharmacology, Emory University School of Medicine, Atlanta, Georgia 30322, and the ^{||}Institute for Biological Resources and Functions, National Institutes of Advanced Industrial Science and Technology, 1-1-1 Higashi, Tsukuba, 305-8566 Japan

Diverse functions of 14-3-3 proteins are directly coupled to their ability to interact with targeted peptide substrates. RSX(pS/pT)XP and RXΦX(pS/pT)XP are two canonical consensus binding motifs for 14-3-3 proteins representing the two common binding modes, modes I and II, between 14-3-3 and internal peptides. Using a genetic selection, we have screened a random peptide library and identified a group of C-terminal motifs, termed SWTY, capable of overriding an endoplasmic reticulum localization signal and redirecting membrane proteins to cell surface. Here we report that the C-terminal SWTY motif, although different from mode I and II consensus, binds tightly to 14-3-3 proteins with a dissociation constant (K_D) of 0.17 μM , comparable with that of internal canonical binding peptides. We show that all residues but proline in -SWTX-COOH are compatible for the interaction and surface expression. Because SWTY-like sequences have been found in native proteins, these results support a broad significance of 14-3-3 interaction with protein C termini. The C-terminal binding consensus, mode III, represents an expansion of the repertoire of 14-3-3-targeted sequences.

The 14-3-3 proteins were initially identified from brain for their abundance and acidic properties (1). They have been found in all eukaryotes and recognized for their diverse functional roles in biological processes including metabolism, cell signaling, intracellular trafficking, stress responses, cell cycle progression, and malignant transformation (see reviews in Refs. 2–4). Multiple isoforms of 14-3-3 are commonly found in a given species. *Saccharomyces cerevisiae* has two 14-3-3 isoforms, encoded by *BMH1* and *BMH2*. Deletion of either does not cause growth defects, but the double deletion of both is lethal in most genetic backgrounds (5–7). Essential to 14-3-3 function, in most cases, is the ability to bind a short peptide substrate only upon phosphorylation. As the first protein module identified with preferential affinity to phosphorylated Ser/Thr substrates, 14-3-3 binding provides an inducible mechanism of translating enzymatic activity to protein-protein interaction, a molecular feature with broad significance in regulation.

Structural studies and examination of the interactive sequences in human proto-oncogene Raf-1 and from random phosphopeptide libraries have established two binding consensuses, RSX(pS/pT)XP and

RXΦX(pS/pT)XP, which are also known as mode I and II recognition (8, 9). The two binding modes have provided molecular insights into the recognition of 14-3-3 binding to a large number of interacting proteins. The vast majority of binding sites identified so far lies internally and matches either mode I or II binding consensus. In addition to phosphorylation-mediated induction of 14-3-3 binding, there is evidence for additional mechanisms of interaction. For example, a tight association between 14-3-3 and multiple regions of plant plasma membrane H^+ -ATPase is induced by additional binding of a fungal toxin, fusicoccin, which leads to the formation of a ternary complex (10, 11). More recently, evidence from studying arylalkylamine *N*-acetyltransferase (AANAT),² the penultimate enzyme in melatonin synthesis, has shown that AANAT has two 14-3-3 binding sites; one high affinity site resides internally, and one low affinity resides at the C terminus. The nonsaturated binary binding of 14-3-3 to these sites was suggested as a tuning mechanism for rhythmic enzyme activity that is coordinated with the daily cycle of melatonin production (12). Both of the above cases involve a low affinity interaction between 14-3-3 and the C terminus: QSYTV-COOH (plant H^+ -ATPase) and RRNSDR-COOH (AANAT). These sequences are distinct and could not have been predicted by the consensus, RSX(pS/pT)XP and RXΦX(pS/pT)XP, in mode I and II binding. The affinity (K_D) for QSYpTV is 2.5 μM , strengthened to 0.027 μM upon ternary binding with fusicoccin (10). The affinity for RRNpSDR is considerably lower than that of the internal canonical binding sequence, and its K_D value remains to be determined (12). This mode of interaction is sufficiently different and thus was recently named mode III (12). It is not well understood whether the interacting C terminus could function independently and whether the reduced affinity is caused by the lack of the conserved proline residue. Information concerning their binding affinity, sequence requirements, and possible selectivity to interact with different 14-3-3 isoforms remain unknown.

We have performed a genetic screen of random peptides to identify C-terminal signal motifs that override endoplasmic reticulum (ER) localization to confer protein expression on cell surface (13). Among the identified motifs is a group of homologous C-terminal peptides that function through an interaction with 14-3-3. Here we report a series of studies to examine the interaction between 14-3-3 and synthetic C-terminal peptides and the ability of the interacting peptides to confer receptor surface expression. The resultant C-terminal peptide consensus expands the repertoire of 14-3-3 recognition motifs and facilitates further functional studies.

* This work was supported by National Institutes of Health Grants GM70959 and NS33324 (to M. L.) and GM53165 and GM60033 (to H. F.) and a predoctoral fellowship award from the American Heart Association (to B. C.). The costs of publication of this article were defrayed in part by the payment of page charges. This article must therefore be hereby marked "advertisement" in accordance with 18 U.S.C. Section 1734 solely to indicate this fact.

¹ To whom correspondence should be addressed: Dept. of Neuroscience, Johns Hopkins University School of Medicine, BRB311, 733 North Broadway, Baltimore, MD 21205. Tel.: 410-614-5131; Fax: 410-614-1001; E-mail: minli@jhmi.edu.

² The abbreviations used are: AANAT, arylalkylamine *N*-acetyltransferase; ER, endoplasmic reticulum; HA, influenza A virus hemagglutinin; Dansyl, 5-dimethylamino-1-naphthalenesulfonyl; PBS, phosphate-buffered saline; Ab, antibody; FAM, 5-(and 6)-carboxyfluorescein; FCM, flow cytometry.

High Affinity Binding of 14-3-3 to Protein C Termini

EXPERIMENTAL PROCEDURES

Molecular Biology—The yeast expression vector for mammalian Kir2.1 was generated by cloning mouse Kir2.1 cDNA in pADNS vector at HindIII and NotI (13). The PstI site was created at the C terminus of Kir2.1 by replacing the last residue with the PstI sequence (LQ). The DNA fragment encoding the C-terminal 36 amino acids of mouse Kir6.2 (LLDALTLASSRGLRKRSVAVAKAKPKFSPDLS) was generated by annealing and extending the complementary oligonucleotides with PstI and NotI overhangs and then ligating to Kir2.1. The SacI site was engineered 9 amino acids downstream of the RKR signal (this caused mutation of PK to EL) to replace SISPDSLS with the DNA fragments encoding the X8 random peptide library. The X8 library DNA fragments were generated by annealing and extending the sense strand (5'-GAGCTCTTT(NNK)₈TAGGCGGCCGCTACATACA, where N indicates any of A, T, C, or G and K indicates either of G or T) and antisense strand (5'-TGTATGTAGCGGCCGCTA) oligonucleotides that were synthesized to randomly encode 8 amino acids preceded by Phe with SacI and NotI overhangs. To clone the CD8 fusion vectors, the cDNA encoding the full-length human CD8 sequence was isolated for fusion with the HA epitope and subcloned into the HindIII-BamHI sites of pCDNA3.1(+) (Invitrogen). The C-terminal 36-amino acid sequence of Kir6.2 was cloned from yeast Kir2.1 fusion vector by PCR with BamHI and EcoRI overhangs and ligated into CD8HA vector at BamHI and EcoRI. A SfiI site was engineered immediately after the SacI site in the 36-amino acid Kir6.2 sequence (LLDALTLASSRGLRKRSVAVAKAKELFSPDLS), causing a substitution of ELF with ELGHLGQ. This SfiI site facilitated replacement of SISPDSLS with the DNA fragments flanking with SfiI and XhoI sites. Mutagenesis of the SWTY sequence was performed by insertion between SfiI and XhoI sites, following extension by Klenow enzyme of oligonucleotides including mutations.

Transfection—The HEK293 cells were transiently transfected using FuGENE 6 (Roche Applied Sciences) and were analyzed at 24–36 h after transfection.

Immunocytochemistry—HEK293 cells plated on polylysine-treated coverslips were transiently transfected. The cells were fixed in 4% paraformaldehyde, PBS for 15 min and permeabilized in 0.05% Triton X-100, PBS for 5 min, all at room temperature. Kir2.1 was detected with mouse anti-HA Ab (Santa Cruz Biotechnologies, Santa Cruz, CA), followed by Alexa Fluor 488-conjugated goat anti-mouse IgG (Molecular Probes, Eugene, OR). The ER marker protein, calreticulin, was detected by rabbit anti-calreticulin Ab (Affinity BioReagents, Golden, CO), followed by Alexa Fluor 568-conjugated goat anti-rabbit IgG (Molecular Probes). The coverslips were mounted on glass slides with Vectashield (Vector Labs, Burlingame, CA), and the images were captured using confocal microscopy. Spinning Nipkow disk confocal microscopy was performed with an UltraView LCI System (PerkinElmer Life Sciences) in conjunction with an Eclipse 200 inverted microscope (Nikon, Melville, NY). Imaging through a 60× oil immersion planar apochromatic lens (numerical aperture, 1.4) was accomplished via excitation using the 488- or 568-nm lines of a krypton/argon laser.

Flow cytometry—The transfected HEK293 cells were harvested by incubation with 0.5 mM EDTA, PBS for 10 min at 37 °C and washed with Hanks' balanced salt solution supplemented with 5 mM HEPES (pH 7.3) and 2% fetal bovine serum (staining medium). All of the incubation and washing steps were performed in staining medium at 4 °C. Surface CD8 was detected with mouse anti-human CD8 monoclonal Ab (Santa Cruz Biotechnologies), followed by Alexa Fluor 488-conjugated goat anti-mouse IgG. The stained cells were examined for surface expression with FACSCalibur (BD Biosciences, San Jose, CA).

Peptide Synthesis and Affinity Measurement—The Dansyl and 5-(and 6)-carboxyfluorescein (FAM)-labeled peptides, Dansyl-RGRSWpTY-COOH, and FAM-RGRSWpTY-COOH, as well as control sequences as RGRSWpTY-COOH, RGRSWTY-COOH, RGRSWpTE-COOH, RGRSWpTD-COOH, RGRSWpTP-COOH, and RGRSWpTG-COOH, were synthesized (New England Peptides, Boston, MA; Abgent, San Diego, CA). The peptide R18, with a sequence of PHCVPRDLSWLD-LEANMCLP, was purchased from Biomol International (Plymouth Meeting, PA). The peptides were prepared as stock solutions by dissolving in water and, if necessary, with the addition of minimal amount of acetonitrile. The working solutions for the affinity detection were prepared in the 10 mM HEPES buffer (pH 7.3).

For detection of both the fluorescence intensity and the fluorescence anisotropy, a multifunctional plate reader Safire² (Tecan US, Research Triangle Park, NC) was used. For fluorescence intensity-based affinity detections with Dansyl-RGRSWpTY-COOH, the excitation was set at 335 nm and emission was set at 545 nm with 20-nm bandwidth for both excitation and emission. The integration time was set at 200 μs with 3 reads/well. The detection was performed on 96-well black microtiter plates with transparent bottoms in top measurement mode. For the fluorescence anisotropy-based affinity measurements with FAM-RGRSWpTY-COOH, the detection was performed with 384-well black microtiter plates in fluorescence polarization measurement mode. The excitation was set at 470 nm and emission was set at 525 nm with 20-nm bandwidth for emission. The time between move and flash was set at 100 ms with 3 reads/well. G-Factor was determined as 1.1 by calibration of 100 nM FAM-RGRSWpTY-COOH as 20 mP for fluorescence polarity, with buffer solution as the reference.

For fluorescence intensity-based affinity detections with Dansyl-RGRSWpTY-COOH, the K_D of Dansyl-RGRSWpTY-COOH with 14-3-3ζ was determined by the titration of 1.2 μM of Dansyl-RGRSWpTY-COOH in 100 μl of total volume with different concentrations of 14-3-3ζ, with one binding site fitting with Equation 1 using Origin 7.0, with $y = F - F_0$, where F is the fluorescence intensity of Dansyl-RGRSWpTY-COOH with the addition of 14-3-3ζ, F_0 is that of Dansyl-RGRSWpTY-COOH alone, and x is the concentration of 14-3-3ζ. Competitive experiments were designed for the K_D measurements of unlabeled control peptides (14). The titrations with different concentrations of Dansyl-RGRSWpTY-COOH were performed with 25 μM of control sequences and 2.65 μM 14-3-3ζ in 100 μl total volume. The fitting was done using Origin 7.0, with the Equations 2, 3, and 4, with $y = F - F_0$, where F is the fluorescence intensity after the addition of Dansyl-RGRSWpTY-COOH to the mixture of control sequences and 14-3-3ζ, F_0 is that of Dansyl-RGRSWpTY-COOH alone in another well without 14-3-3ζ, and x is the concentration of Dansyl-RGRSWpTY.

For fluorescence anisotropy-based affinity detections with FAM-RGRSWpTY-COOH, the K_D value of FAM-RGRSWpTY-COOH with 14-3-3ζ was determined by the titration of 100 nM of FAM-RGRSWpTY-COOH in 100 μl total volume with different concentrations of 14-3-3ζ, with one binding site fitting with Equation 1 using Origin 7.0. In the fitting, $y = r - r_0$, where r is the fluorescence anisotropy of FAM-RGRSWpTY-COOH with the addition of 14-3-3ζ, r_0 is FAM-RGRSWpTY-COOH alone, and x is the concentration of 14-3-3ζ.

For the K_D measurements of unlabeled peptides, competitive anisotropy experiments were performed with the mixture of different concentrations of control sequences with 80 nM FAM-RGRSWpTY-COOH following the addition of 0.65 μM 14-3-3ζ in 100 μl total volume. The fitting was done using Origin 7.0, with Equation 4, and $y = (r - r_0)/(r_{\max} - r_0)$, where r is the fluorescence anisotropy of FAM-RGRSWpTY-COOH with the addition of 14-3-3ζ, r_0 is that of FAM-

RGRSWpTY-COOH alone, r_{\max} is the maximum of fluorescence anisotropy of FAM-RGRSWpTY-COOH with the addition of 14-3-3 ζ , D_0 is the concentration of FAM-RGRSWpTY-COOH, P_0 is the concentration of 14-3-3 ζ , and x is the concentrations of control peptides.

$$y = \frac{Bx}{K_{D_{\text{DansylSWpTY}}} + x} \quad (\text{Eq. 1})$$

$$y = \frac{Bx}{K_{D_{\text{App}}} + x} \quad (\text{Eq. 2})$$

$$K_{D_{\text{App}}} = \left(1 + \frac{[\text{Control}]_0}{K_{D_{\text{Control}}}} \right) K_{D_{\text{DansylSWpTY}}} \quad (\text{Eq. 3})$$

$$y = \frac{1}{2}[D_0] \left\{ \left(\frac{K_{D_{\text{FAM-SWpTY}}}}{K_{D_{\text{Control}}}} x + K_{D_{\text{FAM-SWpTY}}} + [D_0] + [P_0] \right) - \sqrt{\left(\frac{K_{D_{\text{FAM-SWpTY}}}}{K_{D_{\text{Control}}}} x + K_{D_{\text{FAM-SWpTY}}} + [D_0] + [P_0] \right)^2 - 4[D_0][P_0]} \right\} \quad (\text{Eq. 4})$$

Immunoprecipitation and Immunoblot—For immunoprecipitation, transfected cells were washed with PBS once and lysed with lysis buffer (1% Nonidet P-40, 25 mM Tris, 150 mM NaCl, pH 7.50) with protease inhibitor cocktails for 20 min at 4 °C. After spinning for 20 min at 11,000 \times g, the supernatant was mixed with protein A-conjugated agarose beads that were preincubated with 1 μ g of anti-HA Ab (Santa Cruz Biotechnologies). After 5 h of incubation, the beads were washed five times with lysis buffer and then boiled with 2 \times sample buffer for SDS-PAGE analysis.

The samples resolved in SDS-PAGE gels were transferred to nitrocellulose and blotted with anti-14-3-3 Ab (Zymed Laboratories Inc., South San Francisco, CA) or anti-HA Ab (Santa Cruz Biotechnologies), followed by horseradish peroxidase-conjugated secondary antibodies. The immunoblots were developed with the ECL system (Amersham Biosciences).

Expression and Purification of Recombinant 14-3-3 Proteins in *Escherichia coli*—Seven isoforms of 14-3-3 proteins were expressed as hexahistidine-tagged fusions from a T7-driven promoter and purified from *E. coli* strain BL21-SI (Invitrogen). Briefly, *E. coli* BL21-SI cells harboring a 14-3-3 expression vector were grown overnight in salt free LB medium at 30 °C, which was used to inoculate (1%) in a fresh salt free LB medium. When the cell density reached an A_{600} of 0.5, NaCl was added to the final concentration of 0.3 M. The expression of 14-3-3s was induced for 5 h before harvesting. Recombinant His-tagged 14-3-3 proteins were purified using nickel-chelating ion exchange affinity chromatography essentially as previously described (15). Before use, 14-3-3 proteins were subject to gel filtration chromatography using a PD-10 column (Amersham Biosciences) and eluted in HEPES buffer (10 mM, pH 7.3, 130 mM NaCl).

Pull-down of 14-3-3 by Peptides—Purified His-14-3-3 ζ proteins (wild type, K49E, and V176D) were used for the pull-down studies. Specifically, 10 μ M synthetic biotin-conjugated peptides for FRGRSWpTY, FRGRSWTY, and FRGRSWAY (Abgent, San Diego, CA) were incubated with 13 μ M purified 14-3-3 for 30 min at room temperature. The bound material was mixed with streptavidin-Sepharose beads and gently agitated for 1 h. After washing four times with 5% Nonidet P-40 in PBS-T, the beads were resuspended in SDS loading buffer, boiled, and separated by SDS-PAGE followed by Coomassie staining.

SWTX-bound 14-3-3 Homology Modeling—The co-crystal structure of 14-3-3 bound to ARSHpSYPA (a mode I 14-3-3 binding motif) (16) was chosen to model the SWTY motif configuration in the 14-3-3-binding pocket. The electrostatic surface of the 14-3-3 structure (1QJB)

was calculated with the program Pymol (by Warren L. DeLano), as well as the ray tracing. Using the programs O (17, 18) and Quanta (Accelrys, Inc. San Diego, CA), we modeled the sequence of the SWTY motif, RGRSWpTY-COOH, using the mode I peptide amino acids as a template. A radius of 6 Å around the SWpTY peptide was used to manage the contacts. The position of the sequence was anchored by the location of the phosphorylated serine (or threonine) residues in the mode I and the SWTY motif. Homology modeling was repeated for the SWTX panel using the same method.

RESULTS

Affinity Determination of C-terminal Peptides—A typical ER localization signal is capable of dominantly conferring a surface-expressed pro-

tein to ER (19). In a Kir2.1 potassium channel, FCYENE, a cytoplasmic signal, potentiates protein surface expression (20). Addition of the RKR ER localization signal to Kir2.1 prevents surface expression (21). To isolate sequences with ability of overriding the RKR signal and redirecting ER localized proteins to the cell surface, we have constructed a reporter in which constitutive surface expression of Kir2.1 potassium channel protein was abolished by the addition of an RKR ER localization signal (21, 22). Selection of a random 8-mer peptide C-terminal to the

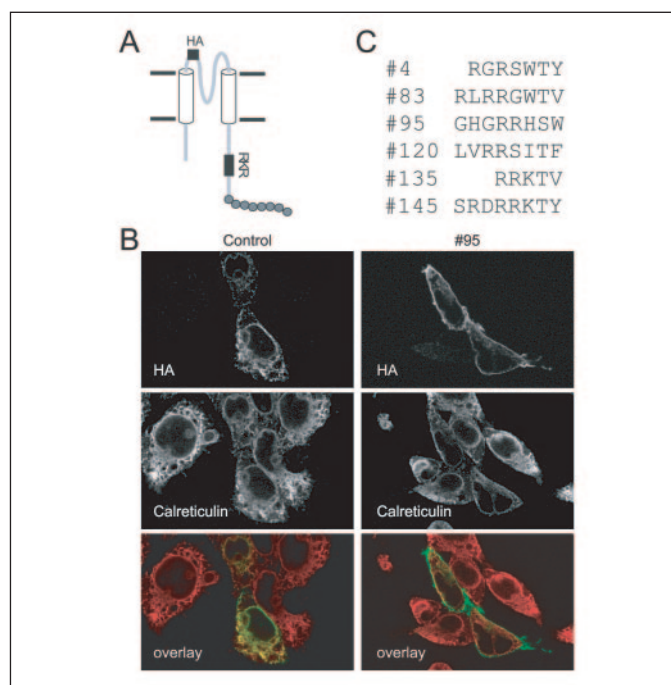


FIGURE 1. C-terminal sequences coding for forward transport. A, a schematic diagram of the Kir2.1 construct used in a yeast screen to identify forward transport signals. Random octameric peptides (X_8) were placed at the C terminus, and 2×10^6 clones were screened for ability to override the ER localization conferred by the RKR motif. B, immunocytochemistry of permeabilized cells transfected with either HA-Kir2.1-GHGRHSW (clone 95) (right panels) or control construct, HA-Kir2.1-SISPDLSL (left panels). The expression of tagged proteins was identified by anti-HA (top panels). The ER morphology was identified by anti-calreticulin (middle panels). The overlay images (green for anti-HA and red for anti-calreticulin) are shown at the bottom. C, amino acid alignment of isolated sequences with both forward transport and 14-3-3 binding capabilities.

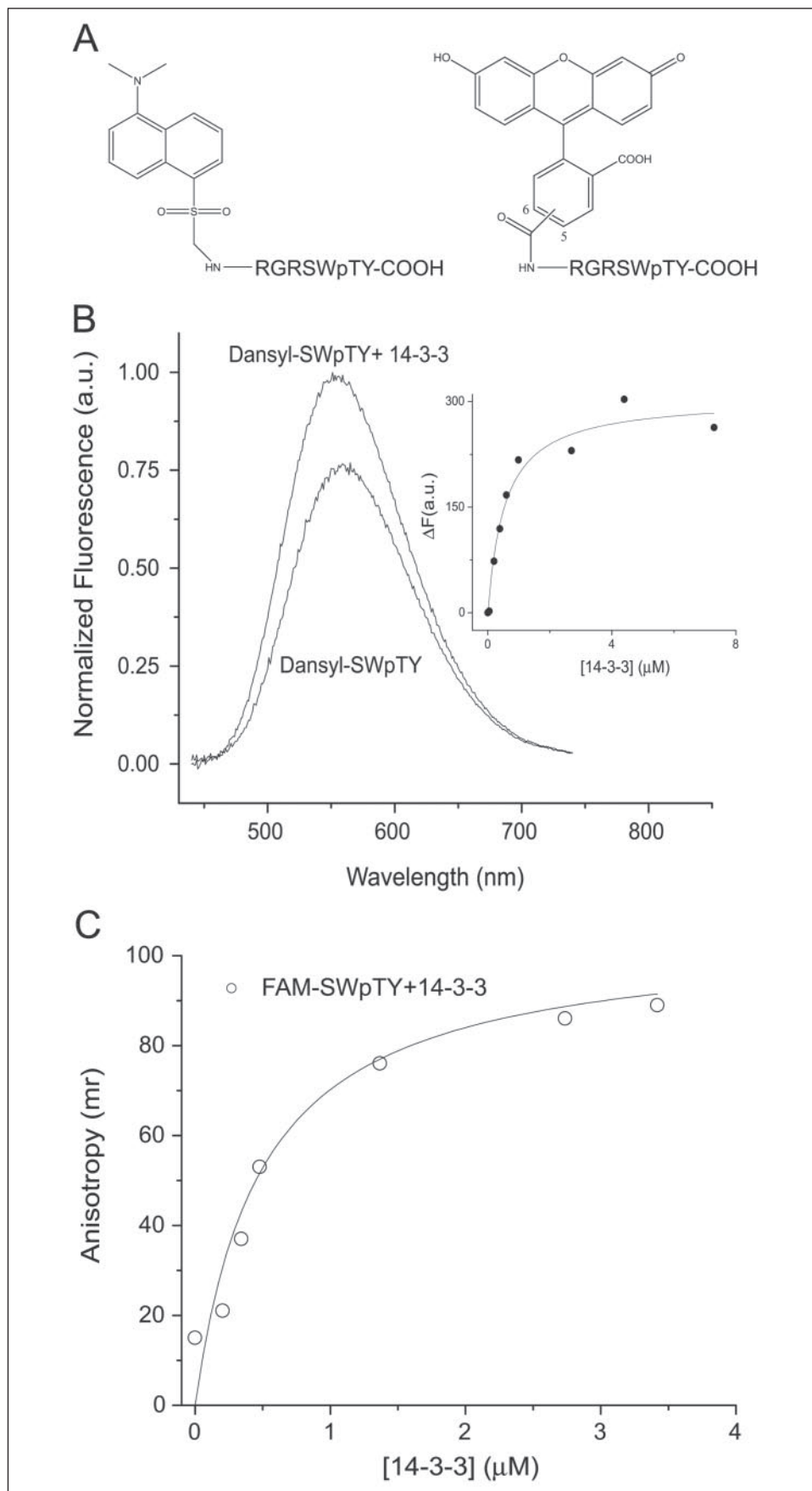


FIGURE 2. **A solution binding assay for measuring 14-3-3 affinity.** *A*, the structures of Dansyl-RGRSWpTY-COOH and FAM-RGRSWpTY-COOH peptide probes. *B*, the emission spectra of Dansyl-RGRSWpTY-COOH alone and saturated with 14-3-3 ζ . The inset is a titration curve representing the change of fluorescence intensity as a function of increasing concentration of purified 14-3-3 ζ . *C*, the anisotropy changes of FAM-RGRSWpTY-COOH are plotted against increasing concentration of purified 14-3-3 ζ . The raw data were fit according to the equations detailed under "Experimental Procedures."

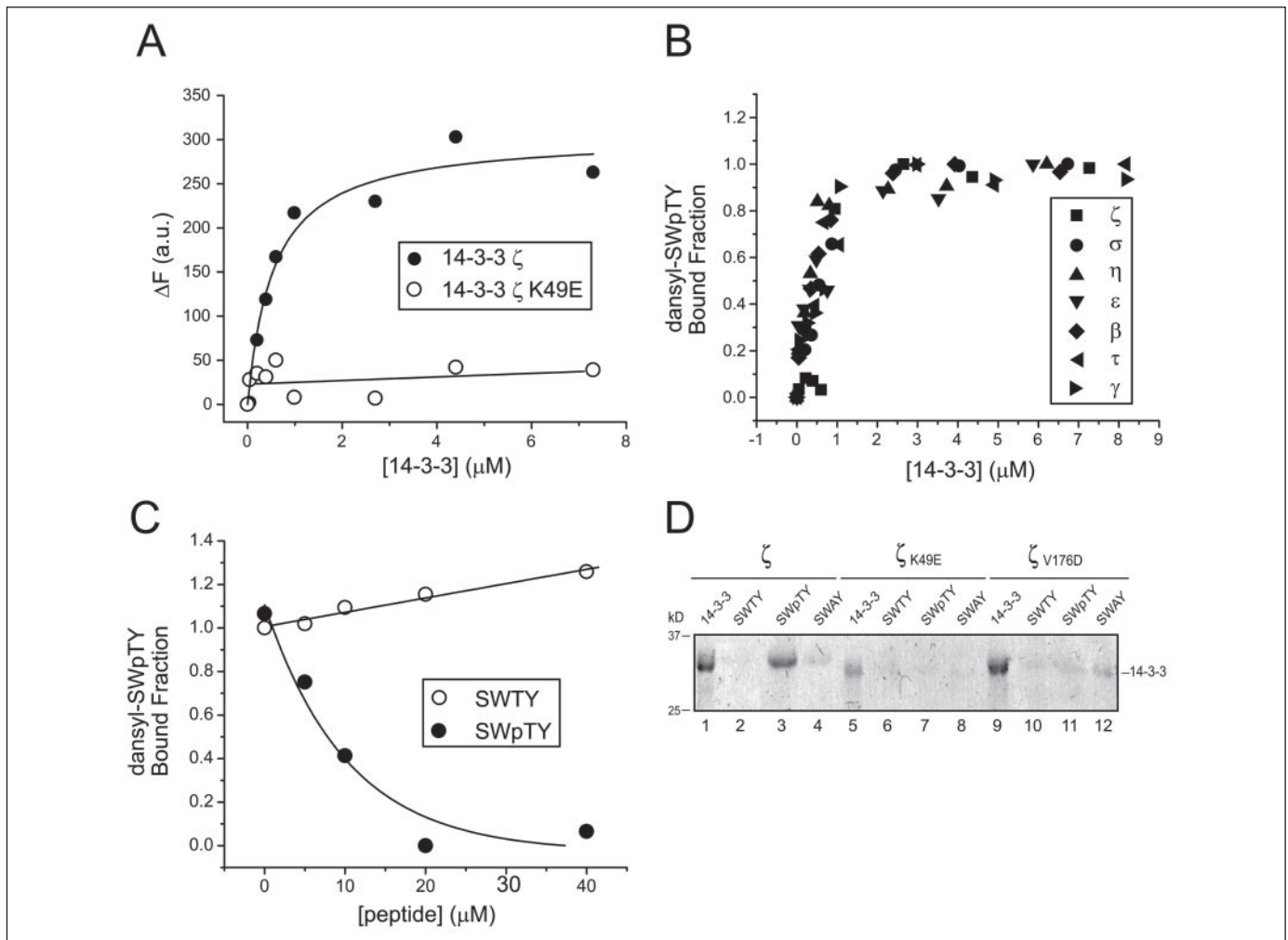


FIGURE 3. Characterization of SWTY motif binding to 14-3-3 ζ . *A*, comparison of affinity for association between Dansyl-RGRSWpTY peptide and 14-3-3 ζ (closed circles) or the mutant 14-3-3 ζ (K49E) (open circles). The change of fluorescence intensity (ΔF , vertical axis) is plotted against concentration of 14-3-3 ζ (horizontal axis). *B*, comparison of binding affinity among different 14-3-3 isoforms. The ΔF values for the 14-3-3 isoforms were individually normalized to calculate the bound fraction (vertical axis) and plotted against concentration of all seven human 14-3-3 isoforms. *C*, competition of 14-3-3 ζ binding by Dansyl-RGRSWpTY-COOH. 14-3-3 ζ was incubated with Dansyl-RGRSWpTY peptide in the presence of increasing concentrations of competitor peptides, RGRSWpTY (closed circles) and RGRSWTY (open circles). The reduction of ΔF values was individually normalized to their maximums to identify the bound fraction. *D*, affinity-precipitation 14-3-3 ζ proteins with synthetic peptides. Biotinylated SWTY, SWpTY, and SWAY peptides were individually incubated with the wild type and K49E and V176D mutants as indicated. Input 14-3-3 proteins are shown in lanes 1, 5, and 9, respectively. The bound materials were precipitated by streptavidin protein A-Sepharose beads and visualized by 12% SDS-PAGE followed by Coomassie staining. The molecular mass standards are as indicated on the left in kDa.

RKR in a yeast genetic system has permitted the isolation of sequences capable of reconferring surface expression by a growth selection (13). In mammalian cells, Kir2.1-RKR was found in ER, co-localized with calreticulin (Fig. 1*B*, left panels). The weak signal on the surface may represent ER compartments in proximity to the cell surface and some Kir2.1 protein escaped from ER localization activity. In contrast, fusion of these sequences to the C terminus, such as GHGRRHSW of clone 95, confers a significant increase of surface expression (Fig. 1*B*, right panels). For the SWTY motif, the ratio of surface/total protein increased by 4-fold compared with that of the wild type (13). We have shown that one group of such sequences achieves their effect via interaction with 14-3-3, and their sequences have several conserved features such as threonine or serine at the -2 position amenable to phosphorylation (Fig. 1*C*) (13). The difference in peptide length was caused by the introduction of a stop codon in the random 8-mer peptide library (see "Experimental Procedures").

The binding between RGRSWpTY-COOH and 14-3-3 has been detected by immunoprecipitation and affinity pull-down using biotinylated synthetic peptide (13). However, like many studies, because of the

dual binding site of dimeric 14-3-3 and involvement of immobilization of peptide ligands on solid surfaces, these binding studies are not most suitable for accurate evaluation of interaction affinity (see "Discussion"). To demonstrate direct and specific interaction with 14-3-3, we developed a fluorescence-based solution binding assay more suitable for affinity quantification with minimal contribution of avidity.

Based on the known structures of 14-3-3, it appears that the binding of the mode I consensus, which SWTY more closely resembles, is no longer selective at the -4 position N-terminal to the phosphorylated residue (16). In addition, the shortest motif isolated from our screen has five residues (Fig. 1*C*, #135). We reasoned that an N-terminal attachment of a fluorophore to the -5 position should be sufficiently distant from affecting the affinity of a binding peptide. Binding of a peptide to 14-3-3 brings the fluorophore to the protein surface and likely geometrically restrains the tethered fluorophore, potentially causing changes of fluorescence intensity and/or polarization (measured as anisotropy).

We synthesized and tested FAM-RGRSWpTY-COOH and 5-dimethylaminonaphthalene-1-sulfonyl Dansyl-RGRSWpTY-COOH (Fig. 2*A*). For the Dansyl-RGRSWpTY, binding to purified recombinant 14-3-3 ζ

High Affinity Binding of 14-3-3 to Protein C Termini

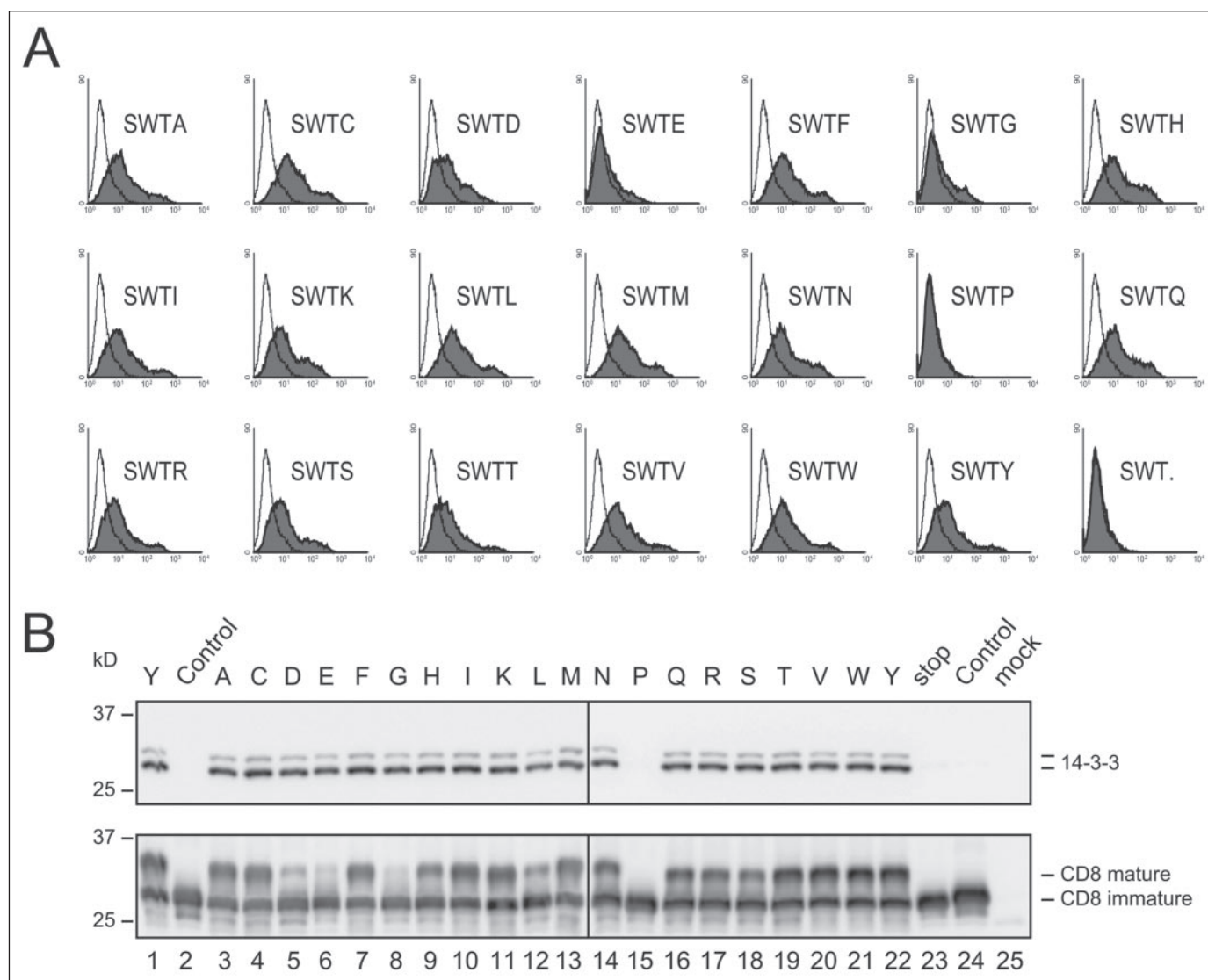


FIGURE 4. FCM and 14-3-3 binding studies of SWTX mutants. *A*, FCM was used to evaluate surface expression of a CD8-RKR-SWTY reporter construct and a panel of SWTX mutants. SWTX FCM histograms display cell number versus logarithmic fluorescence intensity. The negative control (*open areas*) is superimposed with surface expression signal (*filled areas*) of the indicated SWTX sequences. *B*, SWTX mutants are assessed for 14-3-3 binding by co-immunoprecipitation using anti-HA antibody. The *top panel* is blotted with anti-14-3-3 antibody. The *bottom panel* is reblotted with anti-HA antibody to determine the quantity of HA-tagged CD8-RKR-SWTX immunoprecipitated from the total lysates. The negative control construct in *lane 4* is CD8-RKR-SISPDLSL.

potentiates the fluorescence at 545 nm by more than 30% (Fig. 2*B*). No significant fluorescence signal was detected for 14-3-3 protein alone, either wild type or point mutants (Fig. 3*C* and data not shown). For the FAM-RGRSWpTY peptide, we observed a more than 6-fold increase in fluorescence polarization (Fig. 2*C*). These parameters provide a means to monitor the 14-3-3 binding in solution and the ability to compare measurements obtained with two different fluorescence probes (see "Experimental Procedures").

Fig. 2*B* shows the dose-dependent increase of fluorescence intensity for Dansyl-RGRSWpTY-COOH binding to the purified wild type 14-3-3 ζ . When such an increase is fit to a 1:1 bimolecular binding reaction, it gives rise to a K_D of $0.55 \pm 0.12 \mu\text{M}$ between Dansyl-RGRSWpTY and 14-3-3 ζ . Using FAM-RGRSWpTY-COOH peptide and fluorescence anisotropy, we obtained a similar K_D value of $0.49 \pm 0.14 \mu\text{M}$ (Fig. 2*C*). The K_D values in solution are comparable with that of canonical peptide substrates (8). Although it is unknown whether and to what extent the conjugated fluorophores may affect the binding affinity, the similarity of dissociation constants for the two different fluorophore-conjugated

peptides is consistent with the notion of little contribution of fluorophore chemistry to the K_D values (see "Discussion").

C-terminal Peptide Binding Requires the Canonical Binding Groove in 14-3-3—Based on the structure of 14-3-3 with a bound canonical peptide, the Lys⁴⁹ residue forms a critical part of the binding groove. A specific K49E mutation abolished the binding (15). Fig. 3*A* shows the change of fluorescence with increasing concentrations of purified 14-3-3 ζ . Consistent with a specific association with the known 14-3-3 binding groove, an increase of fluorescence intensity was observed from wild type 14-3-3 ζ but not for the mutant 14-3-3 ζ (K49E). There are seven isoforms of 14-3-3 found in human with the potential for isoform-specific functions (23). To examine any isoform selectivity for the SWpTY-mediated interaction with 14-3-3, we expressed and purified each of the seven isoforms from *E. coli* (see "Experimental Procedures"). Under similar experimental conditions, the seven isoforms exhibited similar binding affinity to Dansyl-SWpTY-COOH peptide (Fig. 3*B*). The binding preference was further evaluated through competition with synthetic RGRSWTY and RGRSWpTY peptides. Fig. 3*C* shows that

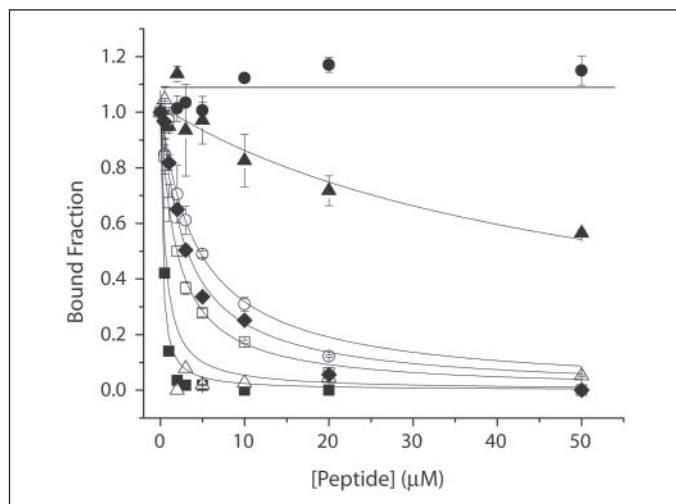


FIGURE 5. Competition anisotropy experiment for affinity measurement of unlabeled synthetic peptides. The detection, done in triplicate, and fittings were performed as described under "Experimental Procedures." ■, SWpTY; ●, SWTY; ▲, SWpTP; ○, SWpTE; □, SWpTG; △, R18; ◆, SWpTD. The resultant dissociation constants are summarized in TABLE ONE.

TABLE ONE

K_D of the peptides with 14-3-3 ζ

Peptide sequences	$K_D \pm$ S.D.
	μM
H ₂ N-RGRSWpTY-COOH ^a	0.17 \pm 0.04
H ₂ N-RGRSWTY-COOH	>100
H ₂ N-RGRSWpTE-COOH	3.4 \pm 0.2
H ₂ N-RGRSWpTP-COOH	45 \pm 11
H ₂ N-RGRSWpTG-COOH	1.5 \pm 0.01
H ₂ N-RGRSWpTD-COOH	2.2 \pm 0.3
H ₂ N-PHCVPRDLSWLDLEANMCLP-COOH	0.39 \pm 0.3

^a pT, phosphorylated threonine.

RGRSWpTY but not RGRSWTY displayed a potent competition, indicating the phosphorylation dependence of 14-3-3 binding to C-terminal peptides. Similarly, using biotinylated peptides of SWTY, SWpTY, and SWAY, we found that only wild type 14-3-3 ζ specifically bound and was precipitated by SWpTY (Fig. 3D, lanes 1–4). In contrast, neither 14-3-3 ζ (K49E) nor 14-3-3 ζ (V176D) was able to bind SWpTY (Fig. 3D, lanes 5–12). Because both of these residues are aligned in the binding groove and necessary for canonical binding to Raf-1 kinase (15, 24), these results support the notion that the phosphorylation-dependent binding to SWpTY peptide is mediated by the same binding groove of 14-3-3 ζ as that for binding canonical peptides.

Selectivity of the C-terminal Residues—The proposed consensus of (pS/pT)_X_{1–2} was based on a few known sequences, but the degeneracy has not been experimentally established (12). Of the different sequences we found to confer surface expression via interaction with 14-3-3, all of them display the preference of a hydrophobic residue at the C-terminal position (pT+1) (Fig. 1C). This raises the question of whether this position is highly selective. To test this possibility, we constructed all 21 variants (SWTX), corresponding to the 20 residues and the stop codon. These mutants are individually expressed using an HA-tagged CD8-RKR-SWTY construct, in which the cell surface expression is directly coupled to the ability of binding to 14-3-3, which overrides the RKR-mediated ER localization and redirects the protein to the cell surface (13). These 21 CD8 fusion proteins were expressed transiently in HEK293 cells, and the surface expression of CD8 was monitored by flow

cytometry (FCM) upon binding to anti-CD8 antibody. Surprisingly, in addition to hydrophobic residues, the C-terminal position was acceptable to most residues of different side chain properties. Notably, both substitution of proline or truncation of the pT+1 residue resulted in complete loss of SWTY function representing the two most intolerable changes. Other changes that were poorly tolerable include two acidic residues (glutamate and aspartate) and glycine (Fig. 4A).

To evaluate the correlation between 14-3-3 binding and surface expression, co-immunoprecipitation was carried out. Consistent with the ability of CD8 surface expression, anti-HA antibody was capable of co-precipitating 14-3-3 for SWTY construct (Fig. 4B, lanes 1 and 22). In contrast, anti-HA was capable of precipitating only immature CD8 in SWTP and SWT expressing cells indicative of little surface expression. Consistent with this idea, it failed to co-precipitate 14-3-3 (Fig. 4B, lanes 15 and 23). The reduced ability to express on the cell surface may stem from differential efficiency in the kinase recognition and/or 14-3-3 binding. To be more definitive, we tested whether SWpTP-COOH is capable of binding to 14-3-3. Peptides corresponding to RGRSWpTD, RGRSWpTE, RGRSWpTG, and RGRSWpTP were synthesized, in which the phosphorylation of threonine was accomplished through chemical synthesis. Using recombinant 14-3-3 ζ and *in vitro* binding analyses, we evaluated their ability to compete with FAM-RGRSWpTY-COOH for binding and measured the K_D values. Fig. 5 shows that RGRSWpTD, RGRSWpTE, and RGRSWpTG were all competitive to FAM-RGRSWpTY-COOH peptide in binding. The K_D values of these peptides correlate with the extent of their ability to confer surface expression (TABLE ONE and Fig. 4). In contrast, RGRSWpTP displayed marked reduction in competing for binding with dissociation constant of 45 \pm 11 μM , ~100-fold reduction of affinity compared with that of RGRSWpTY. Although it could not be determined whether threonine was phosphorylated in the CD8-SWTP construct (Fig. 4, A and B, lane 15), these results show that all but proline are structurally tolerable for SWTX-COOH binding to 14-3-3. Substitution with aspartate, glutamate, and glycine could adversely affect the binding, resulting in ~10-fold reduction in affinity (TABLE ONE). Intriguingly, the random peptide selection for mode I binding showed a preference for both glutamate and aspartate at this +1 position (16) (see "Discussion").

Comparison between SWpTY and a Canonical Binding Consensus—The SWTY sequence differs from the two modes of canonical 14-3-3 binding motifs in that the pT+2 proline is absent from the SWTY motif. In addition, SWTY is functional at the C terminus, whereas the binding motifs for modes I and II are seen to be internal. We constructed a CD8-RKR-SWTP to examine whether the SWTY motif could tolerate an addition of proline after the terminal pT+1 position, thereby transforming SWTY into a mode I-like motif. Judging according to surface expression, CD8-RKR-SWTP displayed an expression level comparable with that of CD8-RKR-SWTY (Fig. 6A). In contrast, substitution of proline with alanine at pT+2 position (*i.e.* SWTYA) greatly reduced the expression level (Fig. 6A). Consistent with flow cytometry data, comparable amounts of CD8 mature form were detected for the SWTY and SWTP constructs, but a much reduced amount of mature form was observed for the SWTYA construct (Fig. 6B, lanes 5 and 6). The apparent subpopulation of higher fluorescence intensity for SWTYA construct is of interest, and similar phenomena were also observed in other constructs (13). The precise mechanism requires further investigation.

It has previously been hypothesized that the function of the proline in the mode I and mode II motifs provides a turn for the bound peptide, hence projecting the subsequent residues out of the binding groove (16). Indeed, the addition of three alanine residues to the C terminus of SWTY abolished the surface expression. By substituting a proline for an

High Affinity Binding of 14-3-3 to Protein C Termini

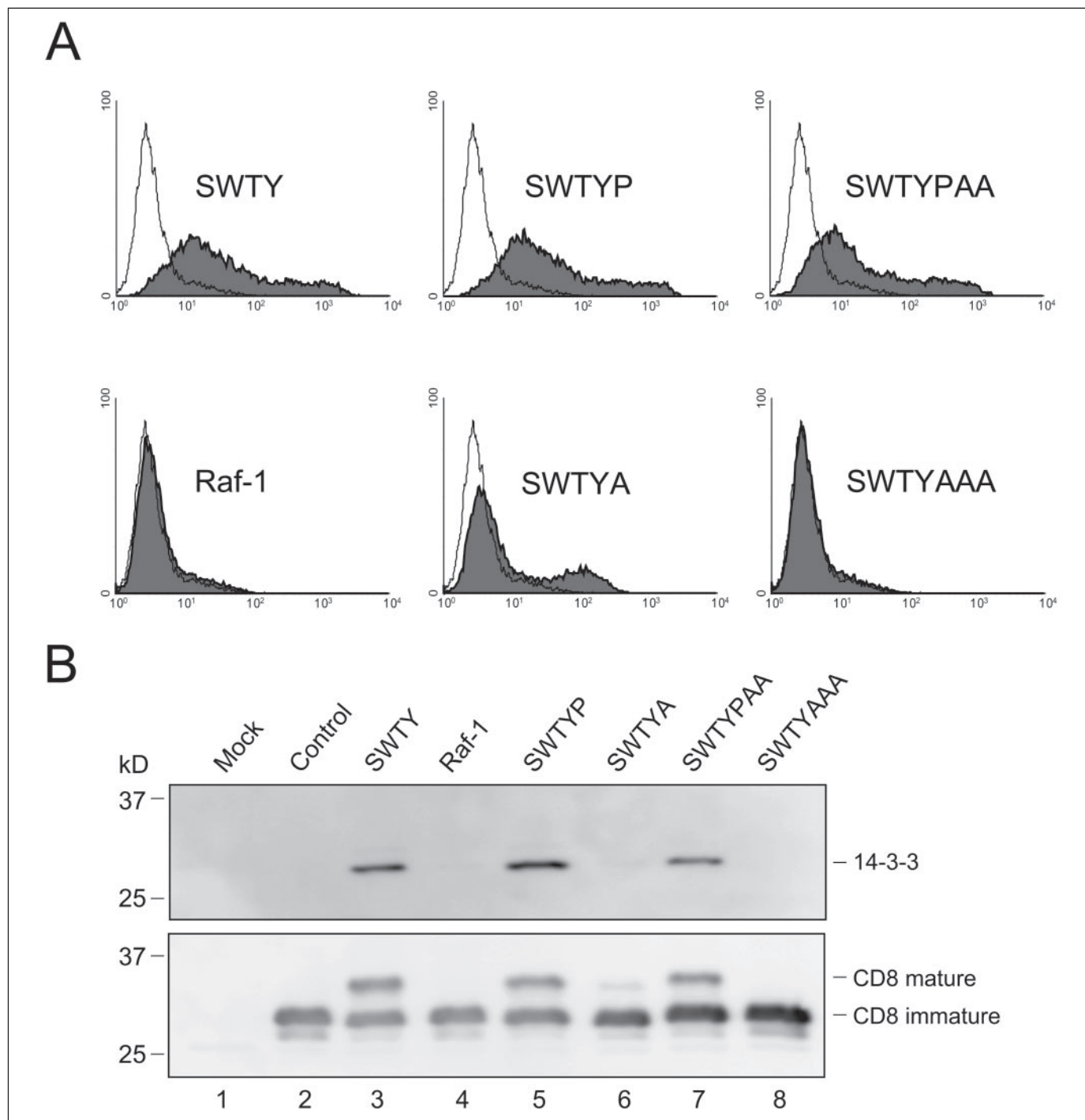


FIGURE 6. Mutagenesis of the SWTY motif. *A*, CD8-RKR-SWTY reporter protein and mutations thereof were measured for surface fluorescence in HEK293 cells. The CD8-RKR-Raf-1 reporter contained the Raf-1 sequence INRSASEP at the C terminus. FCM histograms display cell number versus logarithmic fluorescence intensity. Histograms of the CD8-RKR with indicated sequences are filled with gray and are overlaid with signal of the negative control sequence, SISPDLS. *B*, interactions of 14-3-3 ζ with the indicated motifs were studied by immunoprecipitation by anti-HA. The materials were blotted with anti-14-3-3 (*top panel*) or anti-HA (*bottom panel*). The constructs of different C-terminal sequences are indicated at the top of each lane. The control construct in *lane 2* is CD8-RKR-SISPDLS.

alanine at the pT+2 position, SWTYPAA, both the surface expression and 14-3-3 binding was restored (Fig. 6). This result provides the experimental support for the “turning” hypothesis for proline preference. To test whether a canonical 14-3-3 binding motif similarly functions at the C terminus, we selected the mode I sequence in positions 616–623 of the human Raf-1 protein (INRSASEP), which binds to 14-3-3 in the absence of the second 14-3-3 binding site (25). Expression of the CD8-RKR-Raf1 (INRSASEP) construct, however, failed to promote the sur-

face expression; neither did it confer any detectable 14-3-3 binding as tested by co-immunoprecipitation (Fig. 6). One possible cause for the lack of 14-3-3 binding is the glutamate at the pT+1 position, which is less preferred as shown in Fig. 4 (also see “Discussion”). This experiment provides an example that further supports the distinctive sequence requirements by mode I and C-terminal, mode III, 14-3-3 recognition.

Models of SWTX—Our experiments show that considerable tolerance at the pT+1 position is observed for binding of SWpTX peptides

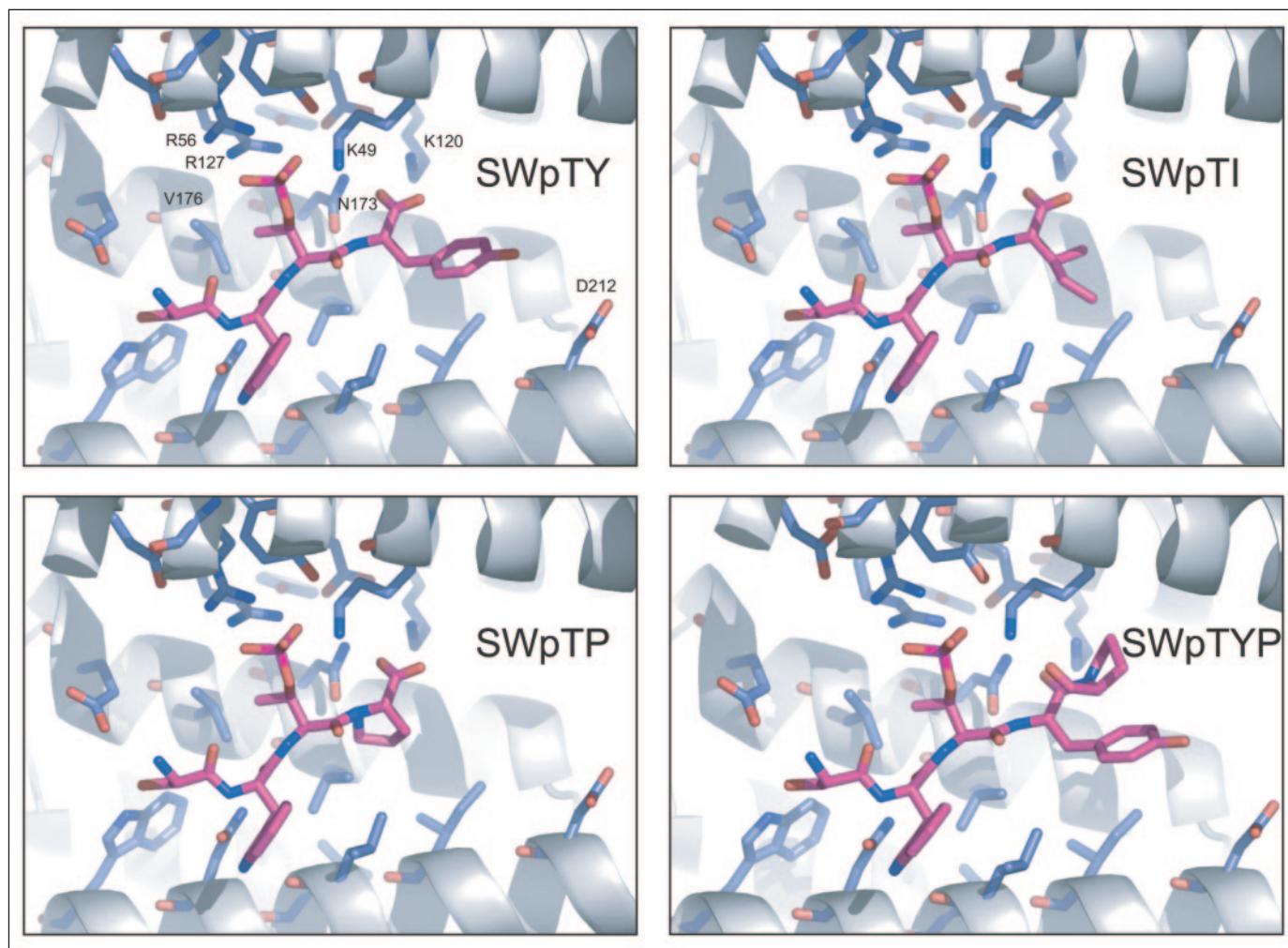


FIGURE 7. **Homology modeling of SWpTY peptides bound to 14-3-3.** Close-up views of SWpTY, SWpTI, SWpTP, and SWpTYP in the binding groove of 14-3-3. The SWpTY peptides are illustrated in magenta, the backbone of 14-3-3 is shown in gray, and the relevant 14-3-3 side chains are shown in blue. The mode I and SWpTY sequences were anchored by the phosphorylated residues.

by 14-3-3; all of the amino acids except proline are allowed (Fig. 4). To learn about the structural basis of this broad specificity, we modeled different SWpTX peptides bound to 14-3-3 using the crystal structure of 14-3-3 with bound mode I peptide ARSHpSYPA (16) as a template, anchoring the position of pT to that of the pS of ARSHpSYPA (see "Experimental Procedures").

Our models show that indeed, there is considerable compatibility allowing acceptance of almost all amino acid side chains. This may be a result of a relatively large binding groove combined with a peptide conformation in which residue pT+1 points away from the groove (Fig. 7, top panels). Lysine 120, conserved in all human, *Drosophila*, and yeast 14-3-3 isoforms, may provide overall stabilization by forming a salt bridge with the terminal carboxylate of the pT+1 residue. Substitution of proline at the pT+1 position would, because of its unique ring structure, lead to a clash between the last backbone nitrogen and the side chain of Asn¹⁷³ of 14-3-3 (Fig. 7, lower left panel). The peptide lacking the pT+1 residue is unable to make the salt bridge to Lys¹²⁰, losing a significant fraction of the stabilization of the complex. Different from the PDZ domain structure, in which the terminal carboxylate group of the substrate was coordinated and pocketed with multiple conserved residues GLGF (26), the 14-3-3 clearly presents a binding groove for which the length of the bound peptide appears to be critical. Longer peptides can be tolerated only if a 90° turn redirects the peptide out of

the binding groove. The presence of a proline residue at position pT+2 may favor such a turn (Fig. 7, lower right panel). This also provides the rationale for progressive reduction of tolerance of alanine C-terminal addition to the pT or pS anchor (Fig. 6).

DISCUSSION

By investigating reporter-based cell surface expression and *in vitro* interactions between synthetic peptides and purified proteins, we found specific association between 14-3-3 and phosphorylated C-terminal peptides. We developed a more accurate solution binding assay allowing rapid determination of affinity for different peptide variants. SWpTY as a member of (pT/pS)_{X₁₋₂}-COOH, also known as the mode III consensus, binds to 14-3-3 with comparable affinity to that of canonical peptides. Our experiments show that all seven human 14-3-3 isoforms are capable of interacting with SWpTY peptides with comparable affinities. With respect to the substrate consensus of mode III, our results provide direct experimental evidence for a broad compatibility of a variety of residues at the pT+1 (C-terminal) position.

In our genetic screen, the identified 14-3-3 binding sequences have two well recognized features: a hydrophobic residue at the C terminus and serine or threonine at the -2 position from C terminus (Fig. 1B). Surprisingly, the SWTX mutagenesis indicated a broad compatibility to all but the proline residue (Fig. 4). The discrepancy may stem from the

High Affinity Binding of 14-3-3 to Protein C Termini

sequential selection by two phosphorylation/14-3-3 binding systems, because the identified clones were first isolated from a yeast growth test and then re-evaluated by a mammalian expression test. Both systems are based on the read-out of steady state surface expression of the reporter protein, a summation of phosphorylation efficiency and 14-3-3 binding affinity (13). When oriented random peptides of MAXXX-pSXXXAKK were screened, the pS(L/E/A/M) preference was proposed (8). Interestingly, a follow-up investigation with a differently oriented synthetic peptide library, MARXXpSXXXAKK, yielded a pS+1 distribution of high abundance for glutamate and aspartate but low abundance for lysine and isoleucine (16). This preference for and against certain residues is different from what was observed in SWTX (Figs. 4 and 5). Furthermore, the binding studies with synthetic peptides showed that the K_D values for RGRSWpTE and RGRSWpTD are 3.4 ± 0.2 and $2.2 \pm 0.3 \mu\text{M}$, respectively, which are about 10-fold lower in affinity compared with RGRSWpTY ($K_D = 0.17 \pm 0.04 \mu\text{M}$) (TABLE ONE). The differential preference at the pT+1 position suggests a possible distinction of mode III binding substrates.

RGRSWpTY-COOH binds to purified 14-3-3 ζ protein with $K_D = 0.17 \pm 0.04 \mu\text{M}$, comparable with the earlier report of a Raf-1 peptide (pS-raf259, RSRSTpSTP), $K_D = 0.51 \mu\text{M}$ by surface plasmon resonance measurement (8). This shows that mode III substrates have the ability to confer canonical binding affinity. Hence, depending on the sequences, mode III binding sites could function in concert with another site as seen in AANAT or H⁺-ATPase (10–12) or function independently without an additional *cis* 14-3-3 site. In addition to AANAT and H⁺-ATPase, C termini of several other proteins were also reported to bind to 14-3-3, including KCNK3 and KCNK9 (27, 28), platelet glycoproteins (29, 30), and nuclear protein p27 (31). The interactions between 14-3-3 and KCNK potassium channels are directly correlated to the surface expression. Although the affinity is yet to be determined, the KCNK sequences are functionally equivalent to SWTY motifs (27).

The RGRSWTY motif could be viewed as a truncated version of a mode I peptide. Consistent with this notion, the extension of SWTY peptide by adding a proline has permitted a strong interaction (Figs. 6 and 7). However, substitution of RGRSWTY with a well characterized mode I motif, INRSASEP of human Raf1, did not confer either 14-3-3 binding or surface expression (Fig. 6), suggesting that mode I sequences are not fully interchangeable with mode III. This could be due to lower affinity because of the glutamate at pT+1 position and/or incompatibility of the C-terminal position with the corresponding kinase.

Using the fluorescence-based solution assay, we have been able to measure K_D values with considerably less material than isothermal titration calorimetry, the other solution based quantification. For both Dansyl-RGRSWpTY-COOH and FAM-RGRSWpTY-COOH peptides, the K_D values (0.55 ± 0.12 and $0.49 \pm 0.14 \mu\text{M}$, respectively) were slightly higher than those determined for nonconjugated peptides using competition assays: $K_D = 0.21 \pm 0.13 \mu\text{M}$ using Dansyl-peptide (data not shown) and $K_D = 0.17 \pm 0.04 \mu\text{M}$ using FAM-peptide (Figs. 2 and 5). The less than 2-fold difference may be caused by the interactions between fluorophores and the 14-3-3 proteins. It should also be noted that our solution-based measurements gave rise to weaker dissociation constants than those obtained with methods involving a solid phase such as affinity pull-down and surface plasmon resonance methods. The K_D of R18 peptide was estimated to be 80 nM by affinity pull-down measurement but 390 nM by fluorescence anisotropy (TABLE ONE) (32). A similar observation was reported for other binding assays using fluorophore-conjugated peptides to probe PDZ domains (14). The fluorescence anisotropy assay using FAM-RGRSWpTY peptide has a high signal to noise ratio. Because the SWpTY motif recognizes the same

binding groove as canonical substrates, the reported probe should be widely applicable to measurements of other 14-3-3 interacting peptides or proteins.

Using the information we have learned in relation to the mode III binding consensus, one can examine potential C-terminal sequence motifs for interaction with 14-3-3. In the human proteome, 15% of proteins have a C terminus with either serine or threonine at the –2 position. Some of them have already shown for 14-3-3 coupled activity. Because they may have differential compatibility for both protein kinase recognition and 14-3-3 binding and because more than one binding site may be present in one complex, a broad spectrum of binding affinities is expected. These represent a significant number of possible 14-3-3 binding sites, hence a considerable expansion of their already abundant roles in biological processes.

Acknowledgments—We thank the members of Li lab for valuable comments and discussions regarding this manuscript.

REFERENCES

1. Moore, B. W., and Perez, V. J. (1967) *Physiological and Biochemical Aspects of Nervous Integration*, pp. 343–359, Prentice-Hall, Englewood Cliffs, NJ
2. Fu, H., Subramanian, R. R., and Masters, S. C. (2000) *Annu. Rev. Pharmacol. Toxicol.* **40**, 617–647
3. Yaffe, M. B. (2002) *FEBS Lett.* **513**, 53–57
4. Dougherty, M. K., and Morrison, D. K. (2004) *J. Cell Sci.* **117**, 1875–1884
5. Roberts, R. L., Mosch, H. U., and Fink, G. R. (1997) *Cell* **89**, 1055–1065
6. van Heusden, G. P., Griffiths, D. J., Ford, J. C., Chin, A. W. T. F., Schrader, P. A., Carr, A. M., and Steensma, H. Y. (1995) *Eur. J. Biochem.* **229**, 45–53
7. Gelperin, D., Weigle, J., Nelson, K., Roseboom, P., Irie, K., Matsumoto, K., and Lemmon, S. (1995) *Proc. Natl. Acad. Sci. U. S. A.* **92**, 11539–11543
8. Yaffe, M. B., Rittinger, K., Volinia, S., Caron, P. R., Aitken, A., Leffers, H., Gamblin, S. J., Smerdon, S. J., and Cantley, L. C. (1997) *Cell* **91**, 961–971
9. Muslin, A. J., Tanner, J. W., Allen, P. M., and Shaw, A. S. (1996) *Cell* **84**, 889–897
10. Wurtele, M., Jelic-Ottmann, C., Wittinghofer, A., and Oecking, C. (2003) *EMBO J.* **22**, 987–994
11. Fuglsang, A. T., Borch, J., Bych, K., Jahn, T. P., Roepstorff, P., and Palmgren, M. G. (2003) *J. Biol. Chem.* **278**, 42266–42272
12. Ganguly, S., Weller, J. L., Ho, A., Chemineau, P., Malpoux, B., and Klein, D. C. (2005) *Proc. Natl. Acad. Sci. U. S. A.* **102**, 1222–1227
13. Shikano, S., Coblitz, B., Sun, H., and Li, M. (2005) *Nat. Cell Biol.* DOI:10.1038/ncb11297
14. Harris, B., Hillier, B., and Lim, W. (2001) *Biochemistry* **40**, 5921–5930
15. Zhang, L., Wang, H., Liu, D., Liddington, R., and Fu, H. (1997) *J. Biol. Chem.* **272**, 13717–13724
16. Rittinger, K., Budman, J., Xu, J., Volinia, S., Cantley, L. C., Smerdon, S. J., Gamblin, S. J., and Yaffe, M. B. (1999) *Mol. Cell* **4**, 153–166
17. Jones, T. A., Zou, J. Y., Cowan, S. W., and Kjeldgaard, M. (1991) *Acta Crystallogr. Sect. A* **47**, 110–119
18. Jones, T. A., and Kjeldgaard, M. (1997) *Methods Enzymol.* **277**, 173–208
19. Jackson, M. R., Nilsson, T., and Peterson, P. A. (1993) *J. Cell Biol.* **121**, 317–333
20. Ma, D., and Jan, L. Y. (2002) *Curr. Opin. Neurobiol.* **12**, 287–292
21. Shikano, S., and Li, M. (2003) *Proc. Natl. Acad. Sci. U. S. A.* **100**, 5783–5788
22. Zerangue, N., Schwappach, B., Jan, Y. N., and Jan, L. Y. (1999) *Neuron* **22**, 537–548
23. Aitken, A., Baxter, H., Dubois, T., Clokie, S., Mackie, S., Mitchell, K., Peden, A., and Zemlickova, E. (2002) *Biochem. Soc. Trans.* **30**, 351–360
24. Wang, H., Zhang, L., Liddington, R., and Fu, H. (1998) *J. Biol. Chem.* **273**, 16297–16304
25. Yip-Schneider, M. T., Miao, W., Lin, A., Barnard, D. S., Tzivion, G., and Marshall, M. S. (2000) *Biochem. J.* **351**, 151–159
26. Doyle, D. A., Lee, A., Lewis, J., Kim, E., Sheng, M., and MacKinnon, R. (1996) *Cell* **85**, 1067–1076
27. O’Kelly, I., Butler, M. H., Zilberberg, N., and Goldstein, S. A. (2002) *Cell* **111**, 577–588
28. Rajan, S., Preisig-Muller, R., Wischmeyer, E., Nehring, R., Hanley, P. J., Renigunta, V., Musset, B., Schlichthorl, G., Derst, C., Karschin, A., and Daut, J. (2002) *J. Physiol.* **545**, 13–26
29. Du, X., Fox, J. E., and Pei, S. (1996) *J. Biol. Chem.* **271**, 7362–7367
30. Andrews, R. K., Harris, S. J., McNally, T., and Berndt, M. C. (1998) *Biochemistry* **37**, 638–647
31. Fujita, N., Sato, S., Katayama, K., and Tsuruo, T. (2002) *J. Biol. Chem.* **277**, 28706–28713
32. Wang, B., Yang, H., Liu, Y. C., Jelinek, T., Zhang, L., Ruoslahti, E., and Fu, H. (1999) *Biochemistry* **38**, 12499–12504